ACS OMEGA

http://pubs.acs.org/journal/acsodf

Article

Molecular Characterization of NSO Compounds and Paleoenvironment Implication for Saline Lacustrine Oil Sands by Positive-Ion Mass Spectrometry Coupled with Fourier-Transform Ion Cyclotron Resonance Mass Spectrometry

Hong Ji,* Sumei Li,* Hongan Zhang, Xiongqi Pang, Yongshui Zhou, and Long Xiang

Cite This: *ACS Omega* 2021, 6, 25680−25691

Read Online

ACCESS | Metrics & More | Article Recommendations

ABSTRACT: NSO compounds mainly exist in geological bodies in the form of nonhydrocarbons and asphaltenes with abundant geological and geochemical information. Combined with the gas chromatography mass spectrometry (GC−MS) technology, positive-ion electrospray ionization Fourier-transform ion cyclotron resonance MS (FT-ICR MS) was used to understand the composition and distribution characteristics of NSO compounds in the oil sands of the Dongpu Depression and to explore their paleoenvironmental significance. The results show that *n*-alkanes are characterized by an even carbon number and phytane dominance, suggesting a saline lacustrine environment. Certain abundance of nC_{37} and β-carotane, high gammacerane content, and low diasterane content are detected in the analyzed samples, reflecting the saline-reducing paleoenvironment for the organic matter. Nine types of heteroatom compounds are detected: N_1, N_1O_1, N_1S_1, O_1, O_1S_1, O_2, O_2S_1, S_1, and S_2. The main compounds are S_1 and N_1 compounds, followed by O_1S_1 compounds. The double-bond equivalent (DBE) value of S_1 compounds is mainly distributed between 3 and 12, and the carbon number is mainly distributed between 18 and 35. The DBE value of N_1 compounds is mainly distributed between 4 and 14, and the carbon number is mainly distributed in the range 15−35. Among the S_1 compounds, DBE_3 compounds (thiophenes) have relatively more sulfur-containing carotenoids (C_{40}). The abundance of C_{40} S_1 and the ratio of pyridine and its homologue DBE_{4-8}/DBE_{9-12} N_1 compounds show a good contrast with the paleoenvironment indicators of gammacerane/C_{30} hopane and diasterane/regular sterane. They can be used as a reference for the paleoenvironment index. Maturity is another factor affecting the distribution of NSO heteroatoms in the oil sands. NSO compounds are enriched in the DBE area with higher condensation, and the main peak carbon shifts forward. As the maturity increases, the relative abundance of N_1 compounds increases, the aromatization intensifies, and carbon is broken into short chains. The research results shed light on the potential application of NSO compounds in petroleum exploration based on FT-ICR MS.

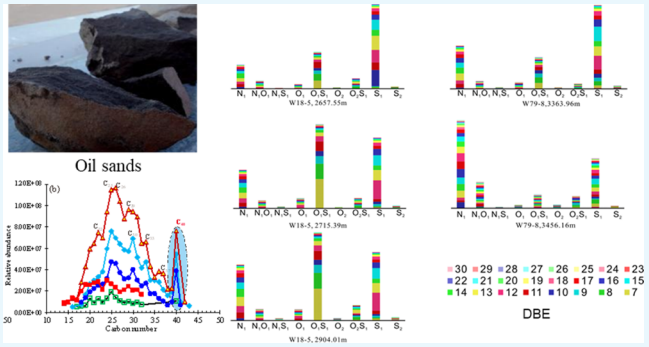

1. INTRODUCTION

Oil sands are sedimentary rocks that contain hydrocarbons such as heavy oil, solid asphalt, and light oil.[1] As an important alternative energy resource for oil and natural gas, oil sands are one of the most important strategic supplements to petroleum resources.[2] Oil sands contain a large amount of nonhydrocarbons and asphaltenes where abundant NSO heteroatom compounds can be detected.[3−5] NSO heteroatom compounds carry rich geological and geochemical information, such as geochemical origins,[3−6] thermal maturity,[7−12] and biodegration.[13,14] Understanding the molecular characteristics of NSO compounds in oil sands is of great significance for further studying the characteristics of oil sands and evaluating the resource potential. However, NSO heteroatom compounds are highly polar compounds with usually low amounts and, therefore, difficult to separate and identify. Conventional technical methods often fail to obtain comprehensive information on heteroatom compounds. At present, the geochemical studies of the NSO compounds are far fewer than those of conventional hydrocarbon compounds. Fourier-transform ion cyclotron resonance mass spectrometry (FT-

Received: July 16, 2021
Accepted: September 9, 2021
Published: September 24, 2021

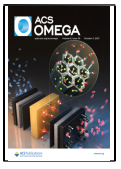

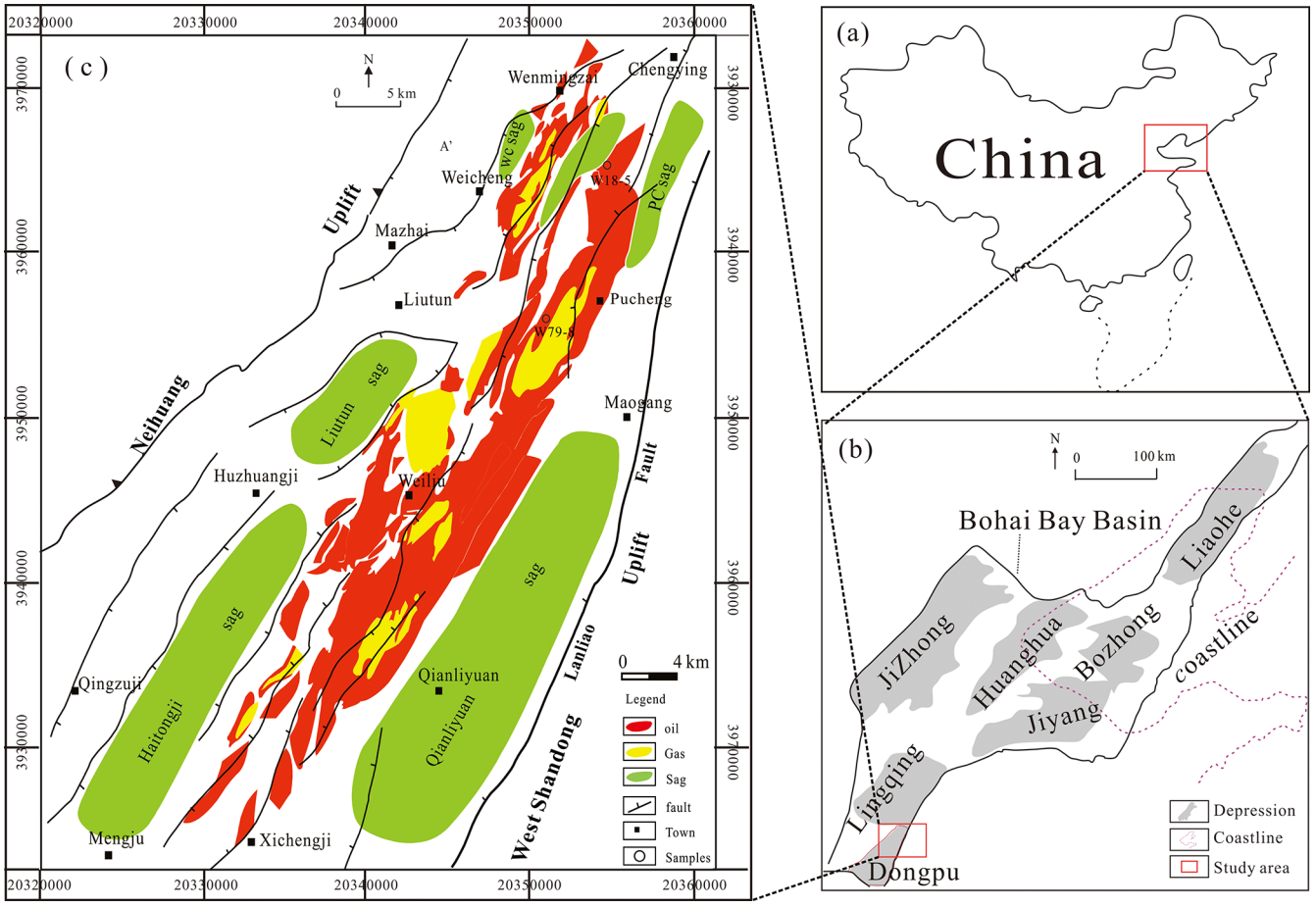

Figure 1. Tectonic units of the Dongpu Depression.

ICR MS) is a new technique introduced in the field of petroleum geochemistry in recent years.[6,7] It has ultra-high resolution and precision and can realize the identification of heteroatomic compounds at a molecular level.

Because of the unique advantages for analyzing heteroatom compounds, using the electrospray ionization (ESI) FT-ICR high-resolution MS technology to study NSO compounds in oil sands is one of the research hot spots in the field of petroleum exploration. Previous studies showed that the distribution characteristics of NSO compounds of oil sands in different areas are quite different,[8,9] and the effects of maturity[10−12] and biodegradation[13,14] affect distributions.[15−17] However, some related factor indexes are mainly based on the analysis technology of negative-ion ESI, and the correlation between positive-ion ESI-related indicators and conventional biomarker parameters has rarely been reported yet.

The Dongpu Depression in the Bohai Bay Basin is one of the most typical saline lacustrine hydrocarbon-generating depressions in China.[12,18,19] Despite its high degree of exploration, the composition and distribution of heteroatomic compounds in the oil sands are unclear, which hinders further exploration in this area. Therefore, in this paper, the FT-ICR MS technique is adopted combined with gas chromatography MS (GC−MS) to reveal the distribution characteristics of heteroatomic compounds in saline lacustrine oil sands and explore their geochemical significance, providing geochemical information for future oil and gas exploration in this area.

2. GEOLOGICAL SETTING

Located in the southeast corner of the Linqing Depression, the Dongpu Depression is an important part of the petroliferous Bohai Bay Basin (Figure 1a,b).[20,21] It is bounded by the Lanliao Fault in the east and the Changyuan Fault in the west (Figure 1c). The southern part of the depression is bounded by the Lankao Uplift, and it is connected to the Kaifeng Depression. The north of the depression is separated by the Maling Fault and is connected to the Xinxiang Depression in the Linqing Depression (Figure 1c). The overall shape of the depression is narrow in the north and wide in the south, with a north−northeast trend (Figure 1c). The Dongpu Depression is based on the Mesozoic and Paleozoic strata, with huge salt-bearing clastic rocks deposited in the Cenozoic (Figure 2).[22,23]

The Cenozoic strata developed the Paleogene Shahejie Formation and the Dongying Formation, and the Neogene developed the Guantao Formation and the Minghuazhen Formation (Figure 2). The Quaternary was deposited in the Pingyuan Formation with a total thickness of about 8000 m. Among them, the Shahejie Formation can be divided into Es_4, Es_3, Es_2, and Es_1; Es_3 is subdivided into lower, middle, and upper members of Es_3, with a stratum thickness of about 1500 m (Figure 2). The details of the stratigraphic characteristics are shown in Figure 2. The Paleogene is composed of the Shahejie Formation and the Dongying Formation, with a thickness of about 6000 m. The Shahejie Formation (Es) is the main target stratum of the oil and source rock, and the overall thickness of the Shahejie Formation is about 5000 m.[24,25]

https://doi.org/10.1021/acsomega.1c03801
ACS Omega 2021, 6, 25680−25691

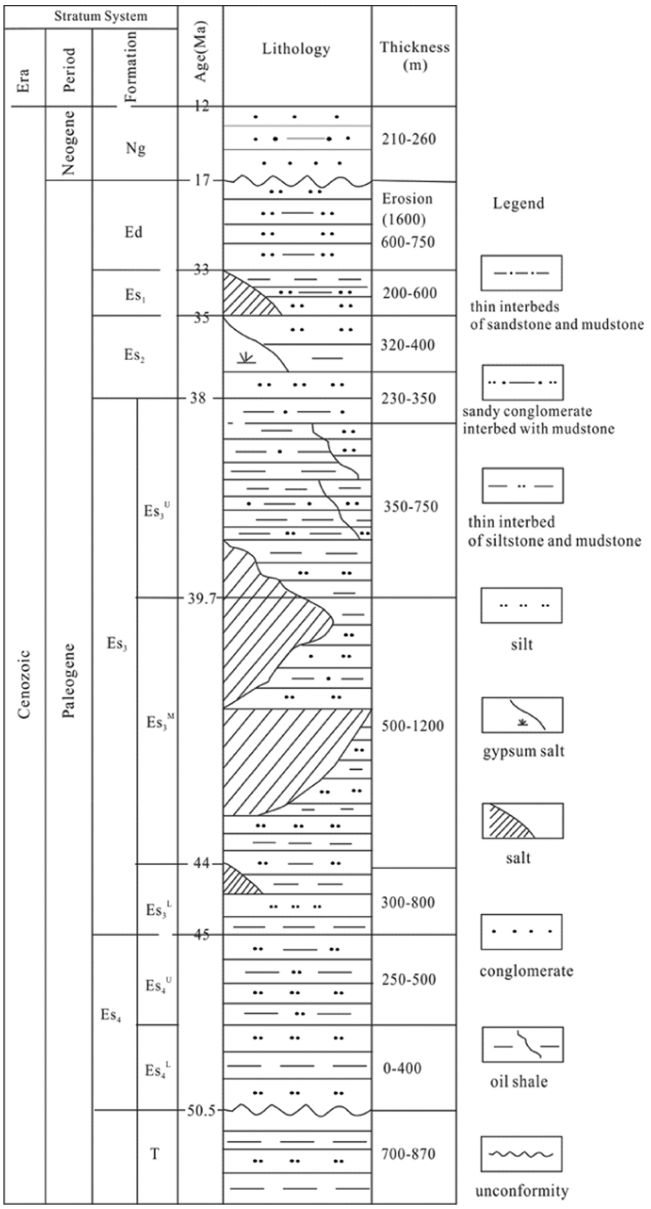

Figure 2. Stratigraphic column showing the nomenclature, thickness, and lithology of major rock units of the Dongpu Depression.

The lithology of each section from north to south varies greatly.[26,27] According to its lithology and fossil combination, the Shahejie Formation is divided into four sections. The fourth member of the Shahejie Formation is divided into two subsections. The third member of the Shahejie Formation is a set of dark reverse-cycle deposits with thin upper and thick lower layers. The central uplift zone can reach 1500−2500 m, and the depth of the depression is more than 3500 m in the third member of the Shahejie Formation (Figure 2). There are three sets of salt deposits in the third member of the Shahejie Formation, which are mainly distributed in Wenliu, Guancheng, Dongying, Wenmingzhai, and Xichengji areas (Figure 2). To the south, there are thin-layer carbonate rocks, oil shale, and sandy mudstone. The second member of the Shahejie Formation is a set of purplish-red and light-brown sandy mudstones deposited in fluvial facies and floodplains, which is a dry lake basin sedimentary environment. The first member of the Shahejie Formation is formed by the subsidence of the basin with lacustrine dark mudstones, sandstones, carbonate rocks, and salt-bearing mudstones. The thickness of the first member is about 250−450 m. The gypsum-salt rocks are mainly distributed in the northern area.[28,29]

3. MATERIALS AND METHODS

Five oil sand samples of different depths and layers were acquired from two wells, W18-5 and W79-8, in the Puwei area of the northern Dongpu Depression (Figure 1c). Three of them are from well W18-5, and the other two samples are from well W79-8. The sample experiment was carried out in the State Key Laboratory of China University of Petroleum (Beijing).

The oil sand sample was manually crushed, and 150−200 g was taken for Soxhlet extraction. Asphaltene is precipitated by *n*-pentane in the oil sand extract and saturated hydrocarbons. Hydrocarbon and nonhydrocarbon components are leached with petroleum ether (60 mL), dichloromethane (about 40 mL), and ethanol (30 mL). The extracts were separated and subjected to GC−MS.

2.1. Whole Oil Analysis. Whole oil analysis was carried out using an Agilent 5890 gas chromatograph equipped with a DB-5 column (30 m × 0.25 mm i.d. and film thickness: 0.25 μm) with H_2 as the carrier gas. The oven temperature was programmed to range from 40 to 310 °C (held 19 min) at 6 °C/min.

2.2. GC−MS Analysis. The extracted saturated hydrocarbons were subjected to GC−MS analysis in the State Key Laboratory of China University of Petroleum (Beijing). GC−MS analysis of the hydrocarbon fractions of the samples isolated by column chromatography was conducted using an Agilent 6890 gas chromatograph with helium as the carrier gas interfaced to an Agilent 59751 mass selective detector. The GC oven temperature for the GC−MS analysis was set to 60 °C for 1 min, then increased to 120 °C at a rate of 4 °C/min and to 300 °C at 2 °C/min, and finally held at 300 °C for 20 min.

2.3. Positive-Ion ESI FT-ICR MS. Bitumen (200 mg) was diluted with 20 mL of dichloromethane (CH_2Cl_2). A total of 50 μL of methyl iodide and 2 mL of silver tetrafluoroborate in 1,2-dichloroethane (20 mg·mL^{-1}) were added to the bitumen solution. The mixture in a beaker was immersed in an ultrasonic bath for 5 min and allowed to react at room temperature for 48 h. The precipitate of silver iodide was removed by centrifugation and then rinsed with CH_2Cl_2. The methyl thiophenium salts and the unreacted oil were obtained by evaporating CH_2Cl_2 from the centrifuged solution. A total of 5 μL of hexane was added to the mixture, and most of the unreacted oil was dissolved in the mixture and separated from the methyl thiophenium salts. Thiophenium salts (10 mg) were diluted with 1 mL of CH_2Cl_2. A total of 5 μL of a thiophenium salt solution was diluted with 1 mL of a toluene/methanol/CH_2Cl_2 (3:3:4) solution.

After the positive-ion methyl derivatization, the 9.4T FT-ICR MS instrument produced by Bruker was used, and the ESI positive-ion mode was selected. The injection speed is 150 L/h, the nozzle voltage is 2.5 kV, and the capillary inlet and outlet voltages are 3.0 kV and 320 V, respectively. The ion source hexapole DC voltage is 2.4 V, the radio frequency is 300V_{p-p}, and the ion storage time is 0.01 s. The ideal mass of Q_1 is 250 Da. The operating conditions of the quadrupole collision cell are 5 MHz, 400V_{p-p}, and the ion storage time is 1 s. The transition time by electrostatic focusing for ion conversion into ICR is 1.3 ms. The working conditions of ICR MS include an

https://doi.org/10.1021/acsomega.1c03801
ACS Omega 2021, 6, 25680−25691

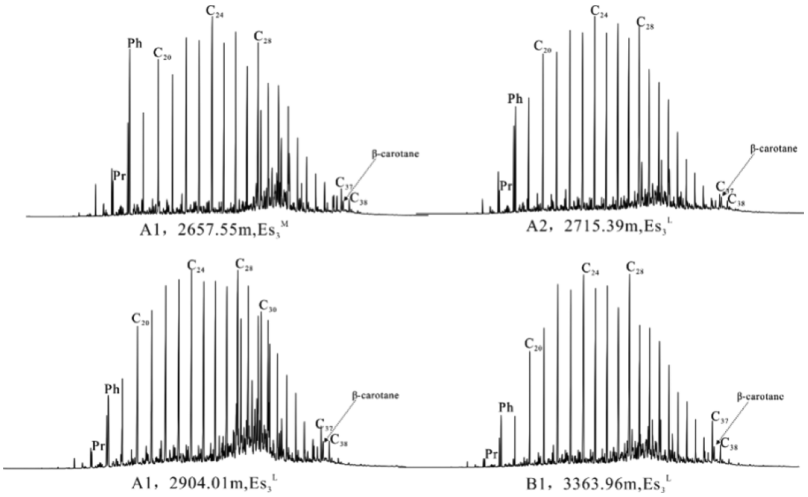

Figure 3. Whole oil chromatographic profiles of selected samples.

Table 1. Geochemical Parameters of the Analyzed Samples[a]

well	W18-5	W18-5	W18-5	W79-8	W79-8
sample no.	A1	A2	A3	B1	B2
depth (m)	2657.55	2715.39	2904.01	3363.96	3456.16
Strata	Es3M	Es3L	Es3L	Es3L	Es3L
CPI	0.86	0.95	0.95	0.88	1.06
OEP	0.84	0.92	0.94	0.90	1.02
Pr/Ph	0.16	0.18	0.16	0.13	0.30
Pr/nC_{17}	1.03	0.75	0.92	1.30	0.54
Ph/nC_{18}	2.73	1.75	1.95	2.79	1.22
C_{21-22}/C_{28-29}	0.79	0.83	0.87	0.71	1.07
$\sum nC21^-/\sum nC22^-$	0.35	0.29	0.24	0.14	0.38
20S	0.34	0.36	0.33	0.52	0.43
$\alpha\beta\beta$	0.30	0.30	0.28	0.40	0.48
$T_s/(T_s + T_m)$	0.21	0.22	0.20	0.17	0.34
dia/reg	0.13	0.16	0.16	0.17	0.31
ste/hop	1.85	1.47	1.70	1.39	1.67
G/C_{30}H	0.76	0.67	0.63	0.97	2.52
C35H/C_{34}H	1.67	1.56	1.49	1.63	0.83
DBTs (%)	20.13	8.92	6.86	8.37	4.66
C_{40}, DBE_3, S_1	6.09	5.63	6.66	4.78	2.55
DBE_{4-8}/DBE_{9-15}, N_1	1.82	1.24	1.37	1.03	0.51

[a]Note: CPI = $[(nC_{23} + nC_{25} + nC_{27}) + (nC_{25} + nC_{27} + nC_{29})]/2 \times (nC_{24} + nC_{26} + nC_{28})$; OEP = $1/4[(nC_{25} + 6nC_{27} + nC_{29})/(nC_{26} + nC_{28})]$; 20S = C_{29}20S/20S + 20R; $\alpha\beta\beta$ = $C_{29}\alpha\alpha\alpha/(\alpha\alpha\alpha + \alpha\beta\beta)$; dia/reg = C_{29} diasterane/sterane; ste/hop = sterane/hopane G/C_{30}H = gammacerane/C_{30} hopane; and DBTs (%) = the content of dibenzothiophene.

excitation attenuation of 11.75 dB, a mass range of 200−750 Da, a data volume of 4M, and the time-domain signal superimposition 64 times. For data processing and analysis, see the literature.[9,14]

4. RESULTS AND DISCUSSION

3.1. Hydrocarbon Characterization by GC−MS.

3.1.1. Whole Oil Analysis. The total-ion chromatogram of the selected sand extracts is shown in Figure 3. The *n*-alkanes for the analyzed samples show even-carbon-number dominance with the carbon number range of 16−40. The carbon preference index (CPI) and odd−even predominance (OEP) values range from 0.86 to 1.02 and 0.84 to 1.02, respectively (Table 1), suggesting some maturity difference. Isoprenoids are rich in bitumens with a strong phytane advantageous distribution (Figure 3), suggesting a saline lacustrine environment. The Pr/Ph ratio ranges from 0.13 to 0.3 with an average of 0.19 (Figure 3, Table 1), suggesting its strongly reducing environment for the organic matter. The ratios of Pr/nC_{17} and Ph/nC_{18} are 0.54−1.3 and 1.22−2.73, respectively (Table 1), indicating that the main source of biogenic input is type II and type III mixed organic matter input. The Pr/nC_{17} and Pr/nC_{18} ratios did not have large differences between the samples, indicating good preservation and low or no biodegradation. A large amount of *β*-carotene was also detected in the bitumens, and the *n*-alkanes were rich in C_{37} and nC_{38} (Figure 3). Studies have shown that the predominance of nC_{37} is mainly controlled by the nature of the depositional environment.[30] The high salinity and strongly reducing depositional environment are responsible for the abundance of nC_{37} in the geological body. In addition, *β*-carotane (Figure 3), which is commonly found in geological samples, usually occurs in an anoxic and strongly reducing saline environment.[31,32] Ding et al. showed that *β*-carotane is mainly derived from the

https://doi.org/10.1021/acsomega.1c03801
ACS Omega 2021, 6, 25680−25691

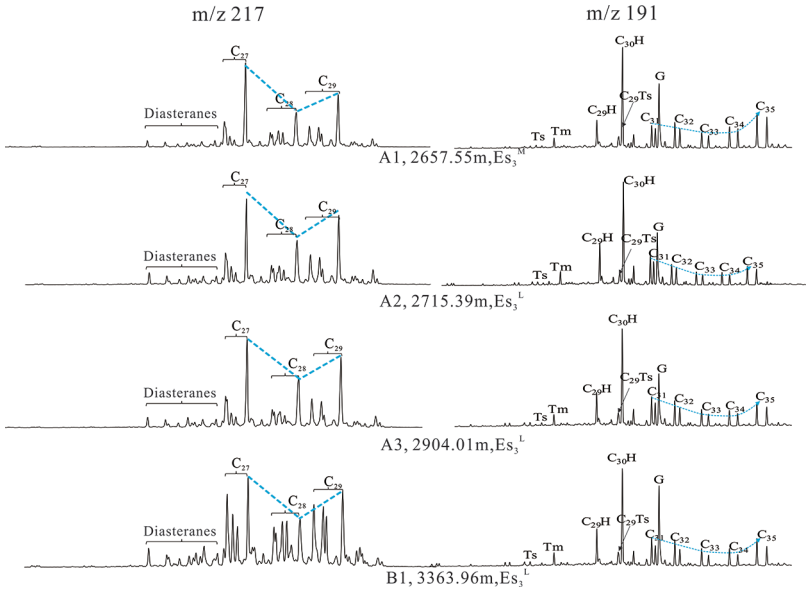

Figure 4. Partial m/z 217 and m/z 191 mass chromatograms showing the distribution of steranes and diasteranes (left) and hopanes (right) on each transect arranged from the least mature (top) to the most mature (bottom). Note: C_{27}, C_{28}, and C_{29} are for C_{27} sterane, C_{28} sterane, and C_{29} sterane, respectively. Ts is for 18α-trisnorhopane; Tm is for 17α-trisnorhopane; H is for 17α(H)hopane; C_{29}Ts is for C_{29} 18α(H)-30 norneohopane; and C_{31}H is for C_{31} 22S/(22S + 22R) homohopane, similarly for C_{32}H, C_{33}H, C_{34}H, and C_{35}H. G is for gammacerane.

terrigenous organic matter and distributed in brackish water conditions in weakly oxidizing to weakly reducing depositional environments.[31] This is consistent with the sedimentary environment of the saline lacustrine facies in the area.

3.1.2. Saturate Biomarker Analysis. The biomarkers sterane and terpanes are detected in the oil sand extract, and representative samples of m/z 217 and m/z 191, respectively, are shown in Figure 4. The selected samples are rich in C_{27}, C_{28}, and C_{29} regular steranes, and the isomerization is relatively low (Figure 4 left). The isomerization ratios of C_{29} $\alpha\alpha\alpha$sterane 20S/(S + R) and C_{29} $\alpha\beta\beta/(\alpha\beta\beta + \alpha\alpha\alpha)$ range from 0.28 to 0.48 and 0.33 to 0.52, respectively (Table 1), suggesting that the oil sands are at less mature to mature stages. The sample of B2 with a deeper depth corresponds to the equilibrium value, proving more mature than other samples (Table 1). The content of diasteranes is relatively low, and the regular sterane is relatively abundant (Figure 4 left). The ratio of diasterane/regular sterane ranges from 0.13 to 0.31 (Table 1). Studies have found that the formation of diasterane is related to the redox properties of the deposition environment.[32,33] In an anoxic and strongly reducing environment with a Pr/Ph of less than 0.5, less diasterane is formed as the carbon skeleton of acidic diasterane is inhibited.[32] Therefore, the low abundance of diasterane and the low ratio of diasterane/regular sterane are also signals of a strongly reducing paleoenvironment for the organic matter. However, there is an outlier diasterane/regular sterane of B2, which shows a higher ratio of diasterane/sterane than others (Table 1). Such cases were also reported in the reducing carbonates which depend on the amount of clay relative to total organic carbon.[32] High diasterane/sterane ratios can result from high thermal maturity as well. Here, in the study area, we deduce that it is the maturity that should be responsible for the higher diasterane/sterane ratio of B2. The sterane/hopane ratios range from 1.39 to 1.85 (Table 1), indicating major contributions from planktonic and/or benthic algae.[32] The terpanes for the analyzed samples show typical characteristics of a saline lacustrine environment. Abundant hopanes were detected, with C_{30} hopane as the main peak (Figure 4 right). High content of gammacerane is notably recognized for the analyzed samples. The ratio of gammacerane/C_{30} hopane ranges from 0.63 to 2.52, with an average of 1.11 (Table 1). Gammacerane is reported to be derived from photosynthetic bacteria and is enriched in crude oil and source rocks from saline lacustrine facies.[32,34] The high abundance of gammacerane is usually associated with brackish water stratification, which shows that the organic matter was originated from the saline and reductive sedimentary environment.[32,34] The hopane in the sample extracts showed an upward-sloping tendency on homohopanes (Figure 4, right). The C_{35}/C_{34} hopane values range from 0.83 to 1.67, with an average value of 1.44 (Table 1), indicating that the original organic matter was originated under a strongly reducing sedimentary environment. A number of thiophene compounds were also detected in the extract, and the abundance of dibenzothiophene compounds was 4.66−20.13% among the aromatic hydrocarbons, with an average of 9.8% (Table 1).

3.2. Characteristics of NSO Compounds Analyzed by FT-ICR MS. *3.2.1. General Distribution Characteristics of NSO Compounds.* The positive-ion ESI FT-ICR MS detected nine types of NSO heteroatom compounds in the oil sands of the Dongpu Depression, including N_1, N_1O_1, N_1S_1, O_1, O_1S_1, O_2, O_2S_1, S_1, and S_2 (Figure 5). S_1, O_1S_1, and N_1 are the main ones, and their relative abundance distributions range from 25.17 to 49.82%, 6.73 to 37.26%, and 13.99 to 44.64%, respectively (Figure 5, Table 2), followed by N_1O_1 and O_2S_1, with their relative abundances in the ranges 3.36−44.64 and 2.71−5.89%, respectively (Figure 5, Table 2). Other types of compounds have lower abundances, usually less than 2% (Figure 5, Table 2). The N_1 groups detected by positive-ion ESI FT-ICR MS are basic nitrogen groups such as pyridine, acridine, or quinoline.[32] It is discovered that with the increase in maturity, the relative content of N_1 compounds increased significantly, from 13.99 to 44.64% (Figure 5, Table 2), indicating the maturity effect on nitrogen compounds.

https://doi.org/10.1021/acsomega.1c03801
ACS Omega 2021, 6, 25680−25691

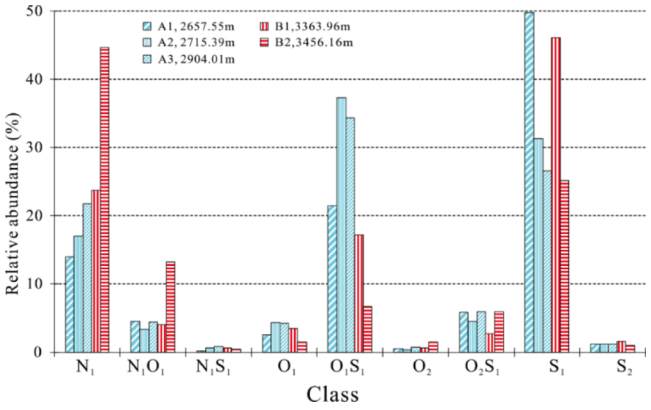

Figure 5. Relative abundance of NSO compounds in oil sands of the Dongpu Depression by ESI (+) FT-ICR MS.

Previous studies have found that nitrogen compounds are sensitive to maturity.[35,36] With the increasing thermal maturity, the contents of various nitrogen compounds in the rock extracts increase drastically, together with significant compositional variations related to alkyl substitution.[37] Although the nitrogen-containing compounds detected by positive ions are basic groups, they are controlled by their maturity and show consistency with the nonbasic "pyrrole-like" nitrogen compounds. The types of NSO compounds detected in the oil sands of the Dongpu Depression are in line with other marine basins or saline facies bodies such as the Tarim Basin,[38] the Alberta area of Canada,[39] and the continental basins developed with saline facies gypsum salt rocks such as the Jianghan Basin[40] and Jinxian Depression.[41] They are all rich in S_1 compounds. However, the relative abundance differences of O_1S_1 and S_2 are different. The compositional differences of NSO compounds may be related to their original source or depositional environment.

3.2.2. S_1 Class Species and Its Geochemical Significance. The S_1 class species is the most abundant species in the sample with a wide range of double-bond equivalent (DBE) and carbon number values. The carbon number and DBE composition and abundance of S_1 compounds in the oil sands of the Dongpu Depression are shown in Figure 6. The carbon number of S_1 ranges from 11 to 50, mainly distributed between 20 and 40 (Figure 6a−e), and the DBE value ranges from 0 to 23, mainly distributed between 4 and 15 (Figure 6f−j). As the maturity increases, the S_1 compounds tend to be enriched in the area with high DBE values. The DBE values in the samples of A1−A3 are mainly distributed in the range 4−12 with the main peaks of DBE being 4 and 6, and the carbon number is mainly distributed in the range 15−35 (Figure 6a−c,f−h), while the DBE values of B1−B2 samples with higher maturity are mainly distributed in the ranges 6−12 and 6−20 with DBE values of 6 and 9 and 12 as the main peaks, respectively, and the carbon number distribution range is much wider within 16−40 (Figure 6d,e,i−j).

It is reported that the DBE value of 0 in the S_1 class species is for alkyl sulfides, while DBE values of 1 and 2 for the S_1 class refer to sulfides with one and two cyclic rings, respectively. Thiophenes have a DBE value of 3.[9] Compounds of DBE values 6, 9, and 12 for the S_1 class are for benzothiophene, dibenzothiophene, and alkyl dibenzothiophene, respectively.[9] The benzo homologue of tetrahydrobenzothiophenes (one aromatic and one naphthenic ring) or phenylthiophene was identified for the DBE value of 7 of the S1 class. DBE values of 9 and 10 of the S_1 class were for the benzo homologues with DBE values of 6 and 7, respectively.[9] As shown in Figure 6, samples with lower maturity for A1−A3 contain less sulfides but higher abundance of benzothiophene compounds (Figure 6a−c,f−h). Benzothiophene (DBE_6 S_1) and dibenzothiophene (DBE_9 S_1) are the most abundant compounds, while sulfides and thiophenes are less abundant in the more mature samples of B1 and B2 (Figure 6d,e,i,j).

The carbon number distributions of DBE values 1, 3, 6, and 9 series compounds are shown in Figure 7. The carbon number of sulfide compounds (DBE_1) ranges from 20 to 33. The carbon number range of samples A1−A3 with lower maturity is much narrower within 15−30, with C_{20} and C_{25} as the main peaks, followed by C_{30}, C_{32}, and C_{33} compounds (Figure 7). However, the distribution of B2 with higher maturity is quite different from others. The carbon number is mainly distributed between 16 and 22, with C_{17} and C_{19} as the main peaks (Figure 7a). The carbon number of thiophene species (DBE_3) is mainly distributed between 22 and 33, with C_{25} and C_{30} as the main peaks (Figure 7b). In addition, thiophenes (DBE_3) contains abnormally high C_{40} and relatively abundant C_{37} (Figure 7b). The carbon numbers of benzothiophenes and dibenzothiophenes (DBE_6 and DBE_9) are mainly distributed in the range of 20−36, with a certain abundance of C_{40} (Figure 7c,d). The more mature sample B2 has a lower abundance in the diabenzothiphene species with the main peaks of C_{14} and C_{15} (Figure 7d).

C_{40} S_1 compounds with various DBE values having high relative abundance are likely to be sulfurized carotenoids that have been found in crude oils.[42] Lexane (C_{33}) was found to be abundant in the oil, which is also present in the desulfurized sulfur fraction (Figure 7b). It is reported that lexane is an important intermediate in the anaerobic thermal degradation of β-carotene.[43] Sulfurized carotenoid C_{40} S_1 compounds with various DBE values are good indicators of the original depositional environment. β-Carotane is highly specific for lacustrine deposition. Under highly reducing conditions, the carbon skeleton of carotenoids exists in the form of β-carotene, associating primarily with anoxic, saline lacustrine or highly restricted marine settings where organisms thrive as the dominant biota.[31,32] Studies have shown that both sulfur complexes and kerogen in high-sulfur crude oil can release β-

Table 2. Relative Abundance of NSO Compounds Detected by Positive-Ion FT-ICR MS

sample no.	depth (m)	Strata	N_1 (%)	N_1O_1 (%)	N_1S_1 (%)	O_1 (%)	O_1S_1 (%)	O_2 (%)	O_2S_1 (%)	S_1 (%)	S_2 (%)
A1	2657.55	Es3M	13.99	4.53	0.16	2.55	21.49	0.48	5.84	49.82	1.14
A2	2715.39	Es3L	17.04	3.36	0.61	4.34	37.26	0.34	4.50	31.32	1.22
A3	2904.01	Es3L	21.73	4.40	0.78	4.22	34.38	0.74	5.91	26.61	1.23
B1	3363.96	Es3L	23.69	4.02	0.64	3.44	17.23	0.66	2.71	46.08	1.54
B2	3456.16	Es3L	44.64	13.21	0.39	1.46	6.73	1.51	5.89	25.17	0.99

https://doi.org/10.1021/acsomega.1c03801
ACS Omega 2021, 6, 25680−25691

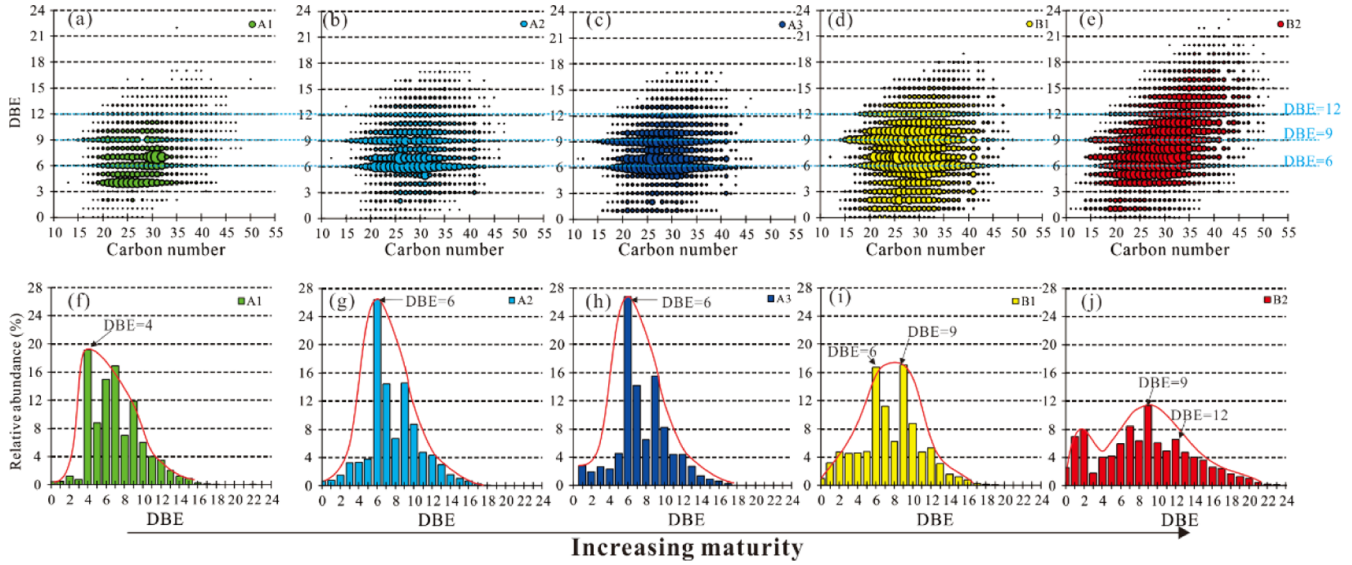

Figure 6. Plots of carbon number vs DBE for the S_1 species (a–e) and relative distribution of the S_1 species with varying DBE values of the selected oil sands (f–j).

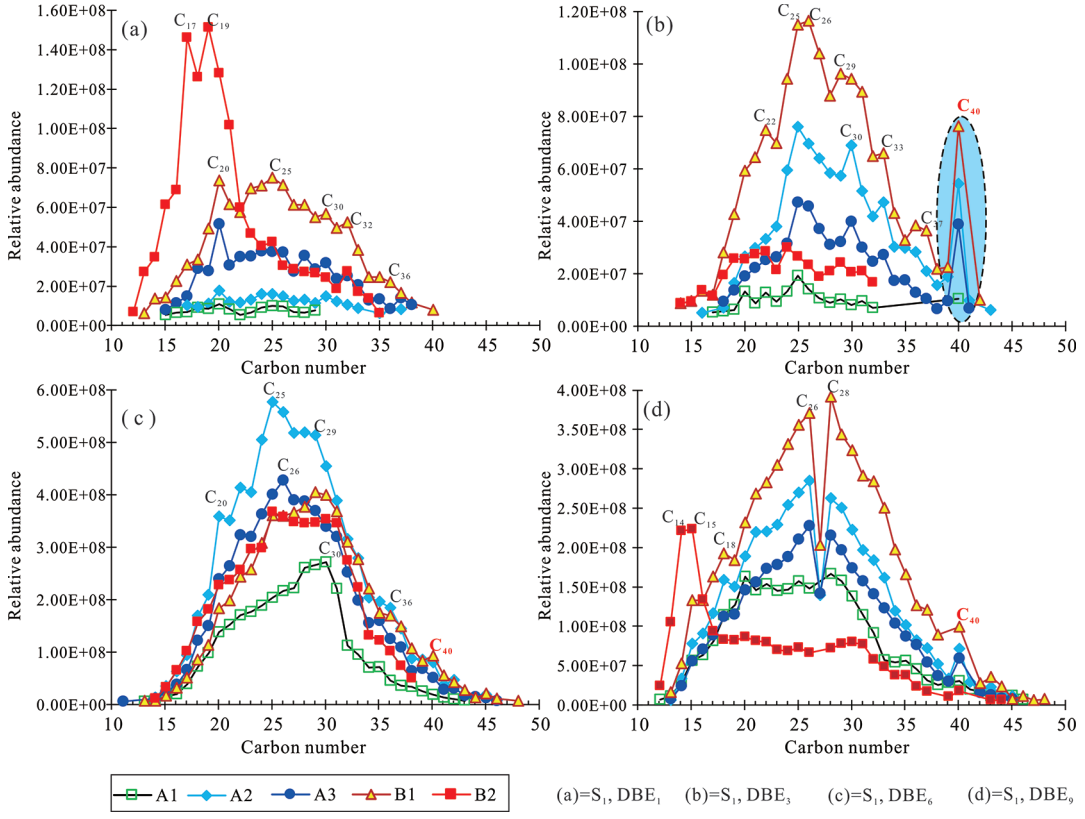

Figure 7. Carbon number distribution and abundance of S_1 compounds with DBE values of 1, 3, 6, and 9.

carotene and other perhydro-carotenoids. This is because in the hypersaline anoxic marine and lacustrine environments, the double bond of β-carotene reacts with sulfur and becomes a component of the sulfur cross-linked system.[32]

The biomarker results show that a low abundance of diasteranes, a high content of gammacerane, and a high homohopane index are signals for a strongly reducing depositional environment. The presence of sulfurized carotenoids in the S_1 species suggests a saline lacustrine depositional setting. This result is also consistent with the high content of β-carotene in the total-ion chromatogram (Figure 3). The correlation variance R^2 of relative abundance between C_{40} sulfurized carotenoids with DBE_3 in S_1 compounds and conventional ratios of diasterane/regular sterane and gammacerane/C_{30} hopane are 0.98 and 0.99, respectively (Figure 8a,b, Table 1). The excellent relationships between the S_1-derived parameters and conventional ratios indicate the application potential of sulfurized carotenoids in sedimentary environmental indicators.

https://doi.org/10.1021/acsomega.1c03801
ACS Omega 2021, 6, 25680−25691

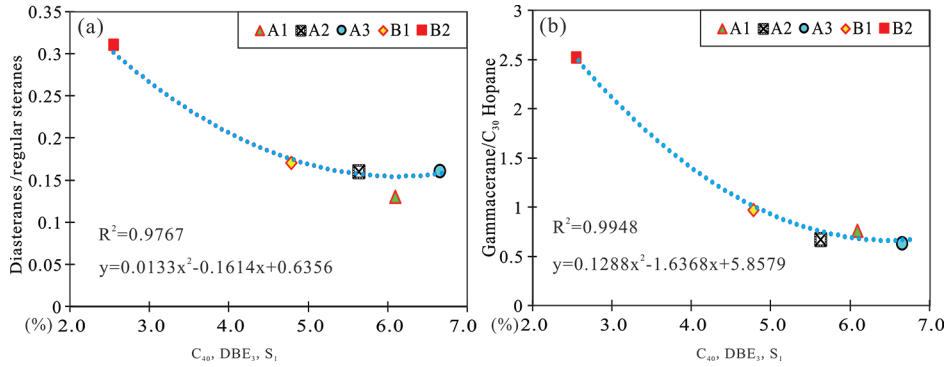

Figure 8. Well correlation between C_{40} DBE_3 S_1 and diasterane/regular sterane (a) and C_{40} DBE_3 S_1 and gammacerane/C_{30} hopane (b).

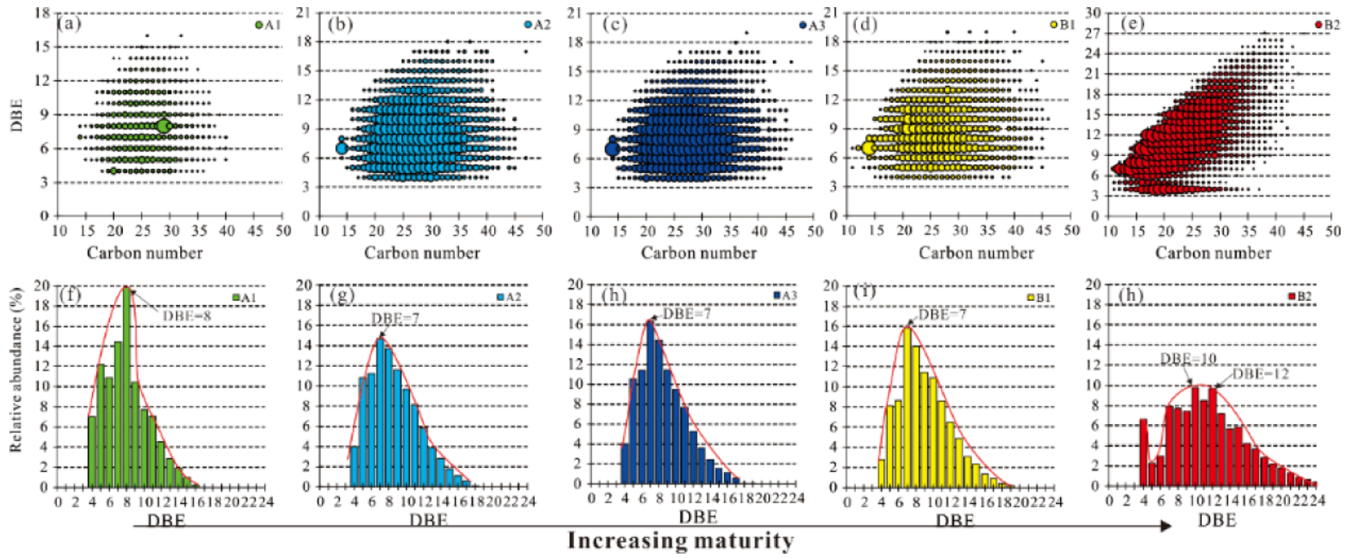

Figure 9. Plots of carbon number vs DBE for the N_1 species (a−e) and relative distribution of the N_1 species with varying DBE values of the selected oil sands (f−j).

3.2.3. N_1 Class Species and Its Geochemical Significance. The carbon number and DBE distributions of the N_1 species in the analyzed samples are shown in Figure 9. The carbon number of the N_1 species is distributed in the range of 10−45, mainly distributed between 18 and 35 (Figure 9). The DBE value distribution ranges from 4 to 24. Samples with lower maturity (A1−A3) show the DBE distribution mainly in the range 4−14, with DBE values of 7 and 8 as the main peaks (Figure 9a−c,f−h). The DBE value of B1−B2 with higher maturity has a wider distribution range within 4−24, with DBE values of 9, 10, and 12 as the main peaks (Figure 9d,e,i−f). As the maturity increases, the carbon number distribution range becomes wider with both lower and higher carbon number compounds, but more compounds are enriched in the DBE value area with a higher condensation degree (Figure 9). The carbon number and DBE distribution of N_1 also reflect the overall impact of the maturity effect.

The carbon number distributions of the main species, the DBE values of 8, 9, 10, and 12, of N_1 compounds are shown in Figure 10. The carbon number is mainly distributed in the range of 10−45, with C_{28} as the main peak (Figure 10). However, the distribution of the B2 sample is quite different from that of other samples due to its maturity (Figure 10). The A1 sample with lower maturity has an absolute predominance of C_{28} in the compound with the DBE value of 8, and the main peaks of other species are C_{20} and C_{28} (Figure 10). The main peaks of carbon of the B2 sample with higher maturity are C_{15} and C_{16}, followed by the secondary main peak of C_{20} (Figure 10), which shows that the N_1 species was affected by maturity. As the maturity increases, the carbon chain is broken, and the main peak of the carbon number moves forward, but the aromatization intensifies (Figure 10).

The N_1 compounds detected by positive-ion ESI were alkylated pyridines and their benzannulated homologues. DBE_7 and DBE_{10} are likely quinolines and benzoquinolines among other pseudohomologues, respectively, according to the positive-ion ESI mode at low maturity.[6,35] At the moderate level of maturity, benzoquinolines and pseudohomologues (DBE_{10}) with a more fully aromatic core structure are presented and become predominant within the heteroatom class, as shown in Figures 9e,h and 10d.

The distributions of the pyridine compounds (N_1) of the analyzed oils are quite different. The distribution difference is also influenced by the depositional environment. Pyridine derivatives are often part of biomolecules such as alkaloids and nucleotides.[44] The depositional environment affects the aromatization and comprehensiveness of pyridine compounds.[45,46] N_1 heteroatom class compounds detected by positive-ion ESI are likely alkylated pyridinic species. DBE values of 5, 7, and 8 represent tetrahydroquinolines, quinolines, and tetrahydroacridines, respectively. Most of the DBE values of 9−15 represent benzoquinolines (DBE_9) and indenoquino-

https://doi.org/10.1021/acsomega.1c03801
ACS Omega 2021, 6, 25680−25691

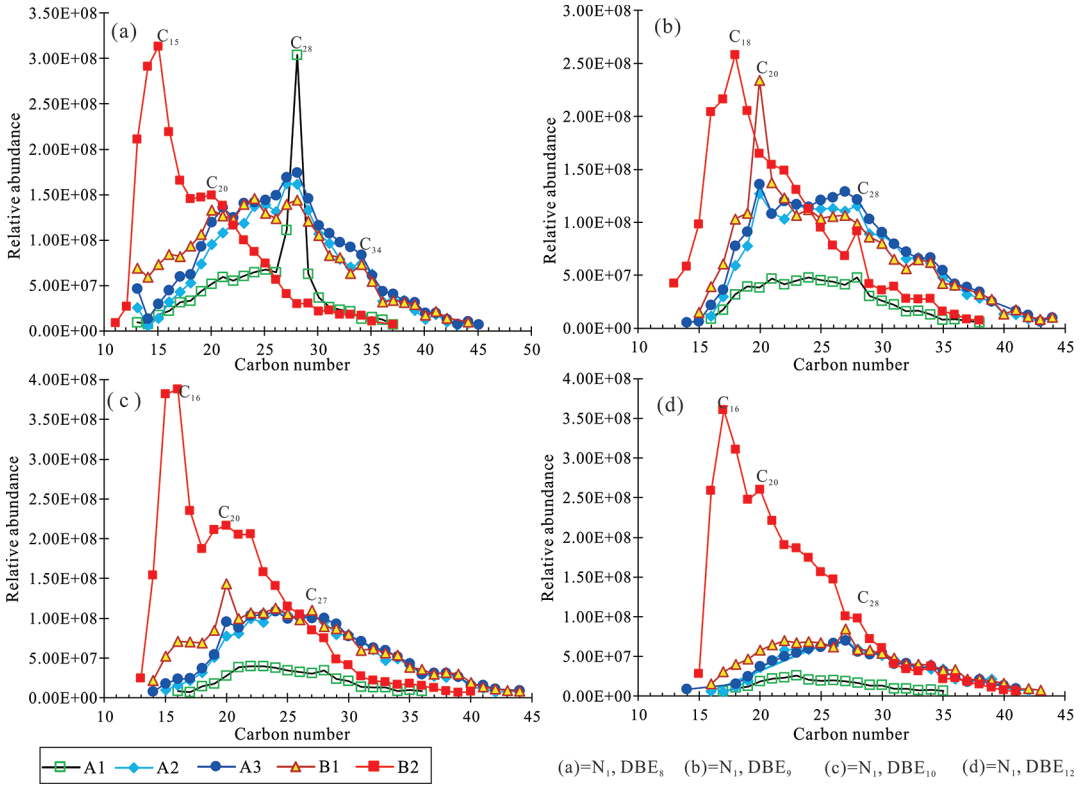

Figure 10. Carbon number distribution and relative abundance of major species DBE_8, DBE_9, DBE_{10}, and DBE_{12} of the N_1 class.

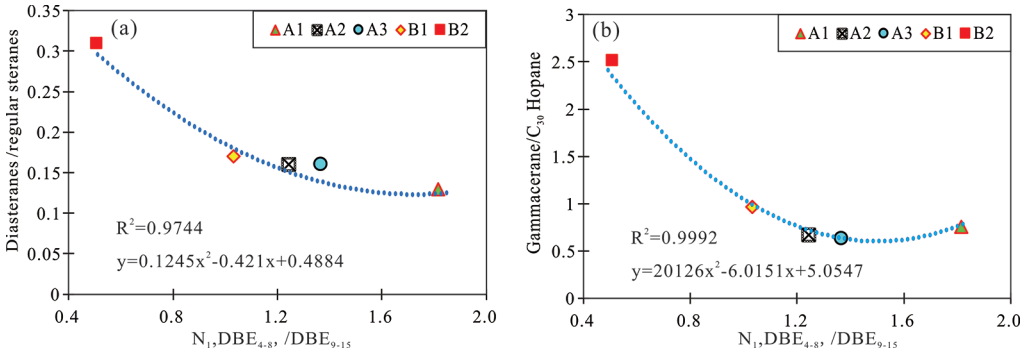

Figure 11. Well correlation between DBE_{4-8}/DBE_{9-15} N_1 species and diasterane/regular sterane (a) and DBE_{4-8}/DBE_{9-15} N_1 species and gammacerane/C_{30} hopane (b).

lines or azopyrenes (DBE_{12}) (Figure 9).[6,35] The study showed that the DBE ratio of DBE_{4-8}/DBE_{9-15} N_1 is well-correlated to the sedimentary environment indicators of diasterane/regular sterane and gammacerane/C_{30} hopane ratios (Figure 11). The correlation value R^2 between N_1, DBE_{4-8}/DBE_{9-15}, and diasterane/regular sterane is 0.9744 (Figure 11a), and the correlation value of R^2 between gammacerane/C_{30} hopane reaches 0.999 (Figure 11b), reflecting that the depositional environment has a significant impact on nitrogen species such as pyridines, benzoquinolines, and pseudohomologues. This result shows that the N_1-derived parameter can be used as potential indicators for paleoenvironmental evaluation.

3.2.4. O_1S_1 Class Species and Its Geochemical Significance. The distribution of O_1S_1 is shown in Figure 12. The DBE values of O_1S_1 in the analyzed samples are distributed between 0 and 21, mainly 1−12, with DBE values of 1, 2, and 5 as the peak species (Figure 12). As the maturity increases, the compounds are enriched in higher DBE values, mainly distributed in the range 7−16 (Figure 12e,j). The carbon number distribution range of O_1S_1 for the analyzed samples is between 11 and 45 (Figure 12). As the maturity increases, the carbon number distribution range narrows (Figure 12e), indicating the maturity control on the NSO compound. In general, what cannot be ignored is that the maturity has an overall impact on the composition and distribution of NSO compounds.

5. CONCLUSIONS

Combined with the GC−MS technology, positive-ion (ESI) FT-ICR MS was adopted to understand the composition and distribution characteristics of NSO compounds in the oil sands of the Dongpu Depression. The geochemical significance of the NSO compounds was explored with conventional GC−MS analysis. The relative abundance of nC_{37} in *n*-alkanes, the appearance of β-carotane, and the high content of gammacerane and C_{35} homohopanes with low content of diasteranes in

https://doi.org/10.1021/acsomega.1c03801
ACS Omega 2021, 6, 25680−25691

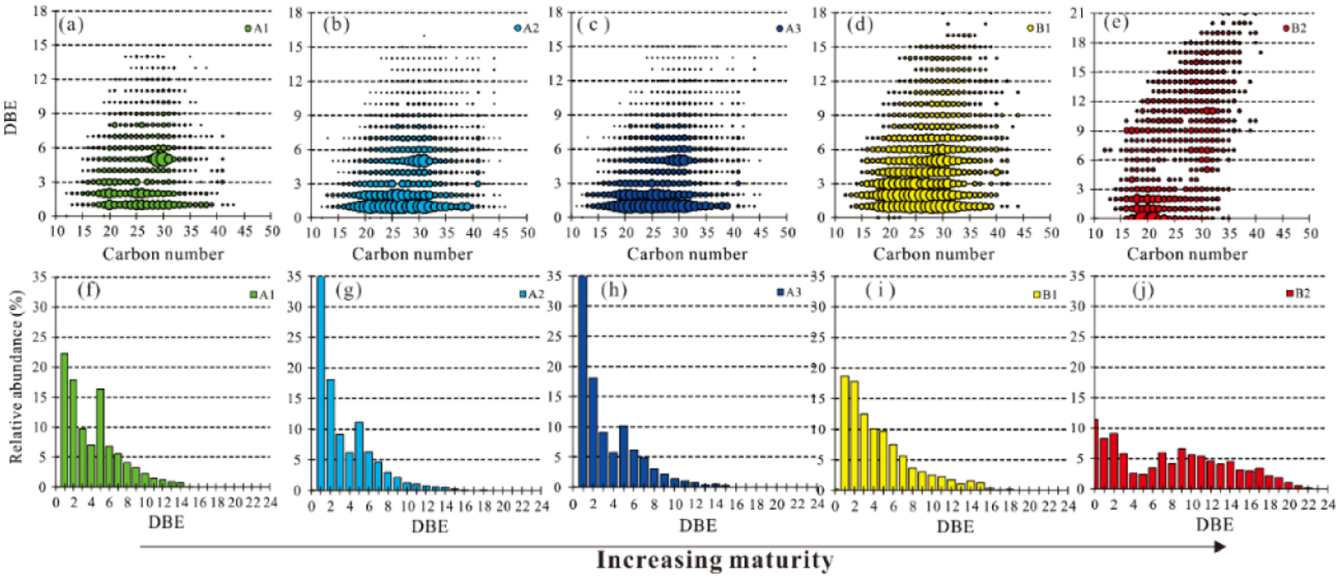

Figure 12. Plots of the carbon number vs DBE for the O_1S_1 species (a–e) and relative distribution of the O_1S_1 species with varying DBE values of the selected oil sands (f–j).

the biomarker indicate that the organic matter derives from strongly reducing and saline lacustrine sedimentary environments. The types of NSO compounds in the oil sand extracts in the Dongpu Depression are complex. Nine types of heteroatom compounds have been detected by positive-ion ESI FT-ICR MS, including N_1, N_1O_1, N_1S_1, O_1, O_1S_1, O_2, O_2S_1, S_1, and S_2. The main compounds are S_1 and N_1 compounds, followed by O_1S_1 compounds. The DBE value of S_1 species is mainly distributed between 3 and 12, and the carbon number is mainly distributed between 18 and 33, which is correlated to the main carbon number distribution of normal alkanes. The DBE value of N_1 compounds is mainly distributed between 4 and 14, and the carbon number is mainly distributed between 15 and 35. Maturity is one main factor affecting the distribution of NSO heteroatoms in the oil sands. As the maturity increases, the relative abundance of N_1 compounds increases. NSO compounds are enriched in the DBE area with higher condensation, and the main peak carbon shifts forward. This is because the maturity increases and the aromatization intensifies, but the carbon chain is broken and reformed. Among the S_1 species, DBE_3 compounds (thiophenes) have relatively high abundance of C_{40} compounds, and their relative abundance has an excellent relationship with the sedimentary environment indicators $G/C_{30}H$ and diasterane/regular sterane. Among the N_1 compounds, DBE_{4-8}/DBE_{9-12} has a good corresponding relationship with the sedimentary environment indexes $G/C_{30}H$ and diasterane/regular sterane. C_{40} DBE_3 S_1 and DBE_{4-8}/DBE_{9-12} N_1 can be used as references for sedimentary environment identification. The research results play an important role in expanding the application of high-resolution MS technology in the field of petroleum exploration.

AUTHOR INFORMATION

Corresponding Authors

Hong Ji − *Guangdong University of Petrochemical Technology, Maoming, Guangdong 525000, China; State Key Laboratory of Organic Geochemistry, GIGCAS, Guangzhou 510640, China; State Key Laboratory of Petroleum Resources and Prospecting, China University of Petroleum, Beijing 102249, China;* orcid.org/0000-0002-5236-7651; Email: jihong@gdupt.edu.cn

Sumei Li − *State Key Laboratory of Petroleum Resources and Prospecting, China University of Petroleum, Beijing 102249, China*; Email: 516343309@qq.com

Authors

Hongan Zhang − *Sinopec Zhongyuan Oilfield Company, Puyang, Henan 457001, China*

Xiongqi Pang − *State Key Laboratory of Petroleum Resources and Prospecting, China University of Petroleum, Beijing 102249, China*

Yongshui Zhou − *Sinopec Zhongyuan Oilfield Company, Puyang, Henan 457001, China*

Long Xiang − *Sinopec Zhongyuan Oilfield Company, Puyang, Henan 457001, China*

Complete contact information is available at: https://pubs.acs.org/10.1021/acsomega.1c03801

Author Contributions

The manuscript was written through the contributions of all authors. All authors have given approval to the final version of the manuscript.

Notes

The authors declare no competing financial interest.

ACKNOWLEDGMENTS

This work was supported by the National Natural Science Foundation of China (2073064), Natural Science Foundation of Guangdong Province, China (20201515110555), State Key Laboratory of Organic Geochemistry, GIGCAS (grant no. SKLOG202014), and Projects of Talents Recruitment of GDUPT (519017). We would like to thank Doctor Cheng and another two anonymous reviewers for constructive comments and helpful suggestions which helped improve the manuscript.

REFERENCES

(1) Jia, C.; Zheng, M.; Zhang, Y. Unconventional hydrocarbon resources in China and the prospect of exploration and development. *Pet. Explor. Dev.* **2012**, *39*, 139−146.

(2) Schramm, L. L.; Stasiuk, E. N.; MacKinnon, M. Surfactants in Athabasca Oil Sands Slurry Conditioning, Flotation Recovery, and Tailings Processes. In *Surfactants: Fundamentals and Applications in the Petroleum Industry*; Schramm, L. L., Ed.; Cambridge University Press: Cambridge, UK, 2000; pp 365−430.
(3) Headley, J. V.; Peru, K. M.; Barrow, M. P. Mass spectrometric characterization of naphthenic acids in environmental samples: a review. *Mass Spectrom. Rev.* **2009**, *28*, 121−134.
(4) Headley, J. V.; Barrow, M. P.; Peru, K. M.; Derrick, P. J. Salting-out effects on the characterization of naphthenic acids from Athabasca oil sands using electrospray ionization. *J. Environ. Sci. Health, Part A: Toxic/Hazard. Subst. Environ. Eng.* **2011**, *46*, 844−854.
(5) Noah, M.; Poetz, S.; Vieth-Hillebrand, A.; Wilkes, H. Detection of Residual Oil-Sand-Derived Organic Material in Developing Soils of Reclamation Sites by Ultra-High-Resolution Mass Spectrometry. *Environ. Sci. Technol.* **2015**, *49*, 6466−6473.
(6) Shi, Q.; Hou, D.; Chung, K. H.; Xu, C.; Zhao, S.; Zhang, Y. Characterization of Heteroatom Compounds in a Crude Oil and Its Saturates, Aromatics, Resins, and Asphaltenes (SARA) and Non-basic Nitrogen Fractions Analyzed by Negative-Ion Electrospray Ionization Fourier Transform Ion Cyclotron Resonance Mass Spectrometry. *Energy Fuels* **2010**, *24*, 2545−2553.
(7) Corilo, Y. E.; Vaz, B. G.; Simas, R. C.; Lopes Nascimento, H. D.; Klitzke, C. F.; Pereira, R. C. L.; Bastos, W. L.; Santos Neto, E. V.; Rodgers, R. P.; Eberlin, M. N. Petroleomics by EASI(±) FT-ICR MS. *Anal. Chem.* **2010**, *82*, 3990−3996.
(8) Miyabayashi, K.; Naito, Y.; Miyake, M. Characterization of Heavy Oil by FT-ICR MS Coupled with Various Ionization Techniques. *J. Jpn. Pet. Inst.* **2009**, *52*, 159−171.
(9) Shi, Q.; Pan, N.; Liu, P.; Chung, K. H.; Zhao, S.; Zhang, Y.; Xu, C. Characterization of Sulfur Compounds in Oilsands Bitumen by Methylation Followed by Positive-Ion Electrospray Ionization and Fourier Transform Ion Cyclotron Resonance Mass Spectrometry. *Energy Fuels* **2010**, *24*, 3014−3019.
(10) Noah, M.; Horsfield, B.; Han, S.; Wang, C. Precise maturity assessment over a broad dynamic range using polycyclic and heterocyclic aromatic compounds. *Org. Geochem.* **2020**, *148*, 104099.
(11) Ziegs, V.; Noah, M.; Poetz, S.; Horsfield, B.; Hartwig, A.; Rinna, J.; Skeie, J. E. Unravelling maturity- and migration-related carbazole and phenol distributions in Central Graben crude oils. *Mar. Pet. Geol.* **2018**, *94*, 114−130.
(12) Ji, H.; Li, S.; Greenwood, P.; Zhang, H.; Pang, X.; Xu, T.; He, N.; Shi, Q. Geochemical characteristics and significance of heteroatom compounds in lacustrine oils of the Dongpu Depression (Bohai Bay Basin, China) by negative-ion Fourier transform ion cyclotron resonance mass spectrometry. *Mar. Pet. Geol.* **2018**, *97*, 568−591.
(13) Liao, Y.; Shi, Q.; Hsu, C. S.; Pan, Y.; Zhang, Y. Distribution of acids and nitrogen-containing compounds in biodegraded oils of the Liaohe Basin by negative ion ESI FT-ICR MS. *Org. Geochem.* **2012**, *47*, 51−65.
(14) Liu, W.; Liao, Y.; Pan, Y.; Jiang, B.; Zeng, Q.; Shi, Q.; Hsu, C. S. Use of ESI FT-ICR MS to investigate molecular transformation in simulated aerobic biodegradation of a sulfur-rich crude oil. *Org. Geochem.* **2018**, *123*, 17−26.
(15) Hughey, C. A.; Rodgers, R. P.; Marshall, A. G.; Qian, K.; Robbins, W. K. Identification of acidic NSO compounds in crude oils of different geochemical origins by negative ion electrospray Fourier transform ion cyclotron resonance mass spectrometry. *Org. Geochem.* **2002**, *33*, 743−759.
(16) Rocha, Y. d. S.; Pereira, R. C. L.; Mendonça Filho, J. G. Geochemical characterization of lacustrine and marine oils from offshore Brazilian sedimentary basins using negative-ion electrospray Fourier transform ion cyclotron resonance mass spectrometry (ESI FTICR-MS). *Org. Geochem.* **2018**, *124*, 29−45.
(17) Orrego-Ruiz, J. A.; Marquez, R. E.; Rojas-Ruiz, F. A. New Insights on Organic Geochemistry Characterization of the Putumayo Basin Using Negative Ion Electrospray Ionization Fourier Transform Ion Cyclotron Resonance Mass Spectrometry. *Energy Fuels* **2020**, *34*, 5281−5292.
(18) Wang, M.; Sherwood, N.; Li, Z.; Lu, S.; Wang, W.; Huang, A.; Peng, J.; Lu, K. Shale oil occurring between salt intervals in the Dongpu Depression, Bohai Bay Basin, China. *Int. J. Coal Geol.* **2015**, *152*, 100−112.
(19) Jiang, Y.-L.; Fang, L.; Liu, J.-D.; Hu, H.-J.; Xu, T.-W. Hydrocarbon charge history of the Paleogene reservoir in the northern Dongpu Depression, Bohai Bay Basin. *Pet. Sci.* **2016**, *13*, 625−641.
(20) Zuo, Y.; Yang, M.; Hao, Q.; Yan, K.; Zhang, Y.; Zhou, Y. New Progress on Hydrocarbon-generation History of the Dongpu Depression in the Bohai Bay Basin based on Thermal History and Hydrocarbon Generation Kinetics. *Acta Geol. Sin.* **2020**, *94*, 1724−1725.
(21) Yan, K.; Zuo, Y.; Yang, M.; Zhou, Y.; Zhang, Y.; Wang, C.; Song, R.; Feng, R.; Feng, Y. Kerogen Pyrolysis Experiment and Hydrocarbon Generation Kinetics in the Dongpu Depression, Bohai Bay Basin, China. *Energy Fuels* **2019**, *33*, 8511−8521.
(22) Tang, X.; Zuo, Y.; Kohn, B.; Li, Y.; Huang, S. Cenozoic thermal history reconstruction of the Dongpu Sag, Bohai Bay Basin: Insights from apatite fission-track thermochronology. *Terra Nova* **2019**, *31*, 159−168.
(23) Zuo, Y.-h.; Ye, B.; Wu, W.-t.; Zhang, Y.-x.; Ma, W.-x.; Tang, S.-l.; Zhou, Y.-s. Present temperature field and Cenozoic thermal history in the Dongpu depression, Bohai Bay Basin, North China. *Mar. Pet. Geol.* **2017**, *88*, 696−711.
(24) Li, X.; Zhang, J.; Xie, J.; Li, C.; Dai, Y.; Li, W.; Zhang, Y.; Li, S. Sedimentary and sequence-stratigraphic characteristics of the lower second submember, Shahejie formation, M1 block, Wenmingzhai oilfield, Dongpu depression, China. *Arabian J. Geosci.* **2015**, *8*, 5397−5406.
(25) Liu, W.; Zhou, X.; Xu, X.; Zhang, S. Formation of inter-salt overpressure fractures and their significances to shale oil and gas: A case study of the third member of Paleogene Shahejie Formation in Dongpu sag, Bohai Bay Basin. *Pet. Explor. Dev.* **2020**, *47*, 560−571.
(26) Wang, Q.; Jiang, F.; Ji, H.; Jiang, S.; Guo, F.; Gong, S.; Wang, Z.; Liu, X.; Li, B.; Chen, Y.; Deng, Q. Differential Enrichment of Organic Matter in Saline Lacustrine Source Rocks in a Rift Basin: A Case Study of Paleogene Source Rocks, Dongpu Depression, Bohai Bay Basin. *Nat. Resour. Res.* **2020**, *29*, 4053−4072.
(27) Huang, C.; Zhang, J.; Hua, W.; Yue, J.; Lu, Y. Sedimentology and lithofacies of lacustrine shale: A case study from the Dongpu sag, Bohai Bay Basin, Eastern China. *J. Nat. Gas Sci. Eng.* **2018**, *60*, 174−189.
(28) Luo, Y.; Liu, H.; Zhao, Y.; Wang, Y.; Zhang, J.; Lü, X. Reevaluation of the origin of overpressure in the inter-salt shale-oil reservoir in Liutun Sag, Dongpu Depression, China. *J. Pet. Sci. Eng.* **2016**, *146*, 1092−1100.
(29) Li, C.; Guo, P.; Liu, C. Deposition models for the widespread Eocene bedded halite in China and their implications for hydrocarbon potential of salt-associated mudstones. *Mar. Pet. Geol.* **2021**, *130*, 105132.
(30) Bao, J.; Zhu, C.; Wang, L. Geochemical characteristic comparison of crude oil samples from the western Qaidam basin. *Oil Gas Geol.* **2010**, *31*, 353−359.
(31) Ding, X.; Gao, C.; Zha, M.; Chen, H.; Su, Y. Depositional environment and factors controlling β-carotane accumulation: A case study from the Jimsar Sag, Junggar Basin, northwestern China. *Palaeogeogr., Palaeoclimatol., Palaeoecol.* **2017**, *485*, 833−842.
(32) Peters, K. E.; Walters, C. C.; Moldowan, J. M. *The Biomarker Guide*, 2nd ed.; Cambridge University Press, Cambridge, 2005; Vol. *1*−*2*.
(33) Zhu, Y.; Zhang, C.; Zhang, M.; Mei, B.; Jin, D.; Xiao, Q. The Effect of Oxidation Reduction Nature of Depositional Environments on the Formation of Diasteranes. *Acta Sedimentol. Sin.* **1997**, *15*, 105−117.
(34) Haven, H. L. T.; Rohmer, M.; Rullkötter, J.; Bisseret, P. Tetrahymanol, the most likely precursor of gammacerane, occurs

https://doi.org/10.1021/acsomega.1c03801
ACS Omega 2021, 6, 25680−25691

ubiquitously in marine sediments. *Geochim. Cosmochim. Acta* **1989**, *53*, 3073−3079.
(35) Oldenburg, T. B. P.; Brown, M.; Bennett, B.; Larter, S. R. The impact of thermal maturity level on the composition of crude oils, assessed using ultra-high resolution mass spectrometry. *Org. Geochem.* **2014**, *75*, 151−168.
(36) Poetz, S.; Horsfield, B.; Wilkes, H. Maturity-Driven Generation and Transformation of Acidic Compounds in the Organic-Rich Posidonia Shale as Revealed by Electrospray Ionization Fourier Transform Ion Cyclotron Resonance Mass Spectrometry. *Energy Fuels* **2014**, *28*, 4877−4888.
(37) Zhang, C.; Zhang, Y.; Cai, C. Maturity effect on carbazole distributions in source rocks from the saline lacustrine settings, the western Qaidam Basin, NW China. *J. Asian Earth Sci.* **2011**, *42*, 1288−1296.
(38) Li, S.; Shi, Q.; Pang, X.; Zhang, B.; Zhang, H. Origin of the unusually high dibenzothiophene oils in Tazhong-4 Oilfield of Tarim Basin and its implication in deep petroleum exploration. *Org. Geochem.* **2012**, *48*, 56−80.
(39) Liu, P.; Li, M.; Jiang, Q.; Cao, T.; Sun, Y. Effect of secondary oil migration distance on composition of acidic NSO compounds in crude oils determined by negative-ion electrospray Fourier transform ion cyclotron resonance mass spectrometry. *Org. Geochem.* **2015**, *78*, 23−31.
(40) Lu, H.; Shi, Q.; Ma, Q.; Shi, Y.; Liu, J.; Sheng, G.; Peng, P. Molecular characterization of sulfur compounds in some specieal sulfur-rich Chinese crude oils by FT-ICR MS. *Sci. China: Earth Sci.* **2014**, *57*, 1158−1167.
(41) Lu, H.; Peng, P.; Hsu, C. S. Geochemical Explication of Sulfur Organics Characterized by Fourier Transform Ion Cyclotron Resonance Mass Spectrometry on Sulfur-Rich Heavy Oils in Jinxian Sag, Bohai Bay Basin, Northern China. *Energy Fuels* **2013**, *27*, 5861−5866.
(42) Wu, J.; Zhang, W.; Ma, C.; Ren, L.; Li, S.; Zhang, Y.; Shi, Q. Separation and characterization of squalene and carotenoids derived sulfides in a low mature crude oil. *Fuel* **2020**, *270*, 117536.
(43) Damsté, J. S. S.; Koopmans, M. P. The fate of carotenoids in sediments: An overview. *Pure Appl. Chem.* **1997**, *69*, 2067−2074.
(44) Newkome, G. R. *The Chemistry of Heterocyclic Compounds: Pyridine and Its Derivatives*; John Wiley & Sons, 2008; Vol. *14*, Part 5.
(45) Bechtel, A.; Gratzer, R.; Linzer, H.-G.; Sachsenhofer, R. F. Influence of migration distance, maturity and facies on the stable isotopic composition of alkanes and on carbazole distributions in oils and source rocks of the Alpine Foreland Basin of Austria. *Org. Geochem.* **2013**, *62*, 74−85.
(46) Zhang, C.; Zhang, Y.; Zhang, M.; Zhao, H.; Cai, C. Carbazole distributions in rocks from non-marine depositional environments. *Org. Geochem.* **2008**, *39*, 868−878.

https://doi.org/10.1021/acsomega.1c03801
ACS Omega 2021, 6, 25680−25691